American Journal of Vehicle Design, 2015, Vol. 3, No. 1, 16-26
Available online at http://pubs.sciepub.com/ajvd/3/1/3

DOI:10.12691/ajvd-3-1-3

On Reducing Sound Reflection and Radiation at Duct Outlet

Sabry Allam*

Automotive Technology Department, Faculty of Industrial Education, Helwan University, P.O. Box 11282-Elkoba, Cairo, Egypt
*Corresponding author: allam@kth.se

Received April 08, 2015; Revised May 15, 2015; Accepted May 26, 2015

Abstract Sound reflection at a duct open end induces resonant amplification of acoustic energy in the duct and causes high intensity sound radiation. This phenomenon sometime causes low frequency noise pollution radiation from pipe and some self-sustained acoustic oscillation in machines. In order to reduce such kind of acoustic resonance, acoustic damping should be added to the duct. Sound reflection coefficient at a duct open end is determined by its outlet shape and wave length. Sometimes a non-reflecting horn with sound absorbing materials is used at the open end in order to realize non-reflecting condition. But, as for low frequency sound, it becomes too huge to be set on real application. In this paper two different outlet shapes; unflanged straight duct and horn that are made of Micro-Perforated Panel (MPP), which can provide wide-band absorption without fibrous and porous materials will be presented. Analytical and 3D Finite element solutions for both cases are presented and used throughout this analysis. The numerical and analytical solutions are compared with measurements and it has been shown that sound reflection and radiation at that open end can be remarkably reduced. The duct side wall next to open end that is made of appropriate MPP plate can reduce the radiated sound up to 5 dB(A) when L/D =10 (pipe length to its diameter). It can be used as an efficient noise control element in automotive intake and exhaust systems.

Keywords: *sound reduction, reflection coefficient, insertion loss, acoustic damping, duct outlet, fem, exhaust system, tail pipe*

Cite This Article: Sabry Allam, "On Reducing Sound Reflection and Radiation at Duct Outlet." *American Journal of Vehicle Design*, vol. 3, no. 1 (2015): 16-26. doi: 10.12691/ajvd-3-1-3.

1. Introduction

1.1. General

Exhaust pipes carrying a mean flow are commonly used in motor cars and aeroplanes. Their acoustical characterizations are therefore important and critical since the acoustic properties of a pipe are significantly affected if a mean flow is introduced and separated at the edge of the pipe exit. Its effect can be clearly seen in the reflection coefficient R for the plane sound pressure waves at the exit to a free field, or to a bigger pipe by a sudden area expansion. When the frequency tends to zero, |R| for the open pipe termination tends to one no matter if there is a mean flow or not. However, when the frequency increases differences occur. Whereas |R| decreases for the quiescent case, it increases to reach a peak greater than one when there is a separating mean flow present. It should be noted that the energy reflection coefficient does not exceed one in any of these experiments [1].

Sound reflection at a pipe open end induces resonant amplification of acoustic energy in the pipe and causes high intensity sound radiation. This phenomenon sometime causes low frequency noise pollution radiated from intake and exhaust systems and some self-sustained acoustic oscillation in machines. In order to reduce such kind of acoustic resonance, acoustic damping should be added in the duct. Sometimes a non-reflecting horn with sound absorbing materials is set at the open end in order to realize non-reflecting condition of sound [2]. But, as for low frequency sound, it becomes too huge to be set on real intake and exhaust systems and machines.

Acoustic liner also increases acoustic damping in the duct, but it is not so effective for absorbing low frequency sound and it is not preferable due to health and environmental legislation requirements. Sound reflection and radiation can be also reduced by using active control techniques [2], but it is not yet practical for real plants due to the real operating conditions. It is noticeable that reflection coefficient is high at the low frequency zone where only plane waves can travel. Then gradual change of wall acoustic impedance is considered to be effective for reducing sound reflection. This phenomenon corresponds to release sound pressure gradually along duct axis. Then the next try is to set tubes with permeable walls next to a duct open end as shown in Figure 1.

Tubes with permeable walls are used in various applications, one of which is in the intake systems of internal combustion (IC) engines, where the tube is placed upstream of the air filter. A typical such tube might be made from wire-reinforced woven fabric or similar perforated/micro perforated elements. An understanding of sound propagation in permeable tubes is clearly desirable in the development of predictive design for

engine intake systems. Also, it is often used as a key element in most of silencing systems. The porosity nature of the tube walls renders the internal wall impedance is complex, so that an internally propagated sound field will be axially attenuated. But it can also introduce significant acoustic coupling between the interior and the exterior of the duct, and this feature distinguishes permeable-walled ducts from other types of soft-walled duct, in which internal/external acoustic coupling is usually minimal. For example, unlined ducts with impermeable but flexible walls radiate internal noise to the exterior via internally excited wall vibration [3,4], but this tends to occur principally in narrow frequency bands around structural resonances of the walls.

In unlined sheet metal ducts, coupling between wall vibration and the external sound field is usually weak and may be neglected [5]. In acoustically lined sheet metal ducts, the walls are usually sufficiently massive to inhibit internal/external sound transmission, though Cummings and Astley [6] have shown that this can be significant in the case of rectangular ducts with lightweight walls, where coupling between wall vibration and the internal sound field also needs to be taken into account.

Cummings and Kirby [7] presented a predictive model for sound propagation in tubes with permeable walls. Acoustic coupling between the internal and external sound fields is taken into account by the use of an iterative procedure that involves finite-length of uniform properties in the tube and an appropriate external radiation model. The propagation model is verified by comparison to experimental data on a perforated metal tube and is applied to a practical type of permeable fabric tube. Good agreement between prediction and experiment but their procedure is complicated.

Dokumaci [8] studied the pipes with porous walls, he proposed an integro-differential system for the propagation of plane sound waves in pipes with porous walls, and presents its general numerical solution, as well as an approximate analytical solution. The predicted effect of the coupling between the internal and external acoustic fields in a circular pipe made of reinforced woven fabric walls is shown. This proposed solution is very complex and is not so easy to be implemented by acoustic engineers and junior researchers.

In this paper within a small Helmholtz number (ka), where k is the wave number and a, is the duct radius, new concepts which can be easily used by acoustic engineers to reduce the sound reflection coefficient and sound radiation at a duct open end are presented. When a duct side wall next to open end is made of appropriate micro perforated (MPP) or perforated plates, which has hard wall duct the acoustic coupling between inner and outer domains of the pipe is performed using the wall impedance and the wall vibration is very week and can be safe neglected. Here this phenomenon is analyzed theoretically, numerically, and validated experimentally and practically on the real vehicle. All design parameters are investigated. A simple application of the proposed element is tested on real vehicle and compared with the theoretically predicted. This technique is useful and can be applicable to reduce acoustic resonant intensity in ducts such as engine intake and exhaust systems and stacks of plants.

1.2. Structure of the Paper

In section 2, theoretical models; 1D, 2D based models and FEM for sound transmission in straight duct with permeable walls are firstly derived and used to study the effect of different design parameters on reflection coefficient and sound radiation at duct termination. In all models the inner and outer domains of the pipe are coupled through wall impedance. Theoretical results that present the effect of all design parameters are also presented in section 2.

To validate the presented models and the new concept of reflection coefficient reduction, an experimental test set up is introduced in section 3, reflection coefficient measurement procedure is presented, a comparison between predicted and measured reflection coefficient are also presented in section 3. Practical application for using the test object as passenger car tail pipe is presented as well.

The application of the same theoretical and numerical procedure to a conical test object is introduced in section 4. A comparison between the predicted reflection coefficient for conical and straight pipe with the same length is also introduced in section 4. Conclusion and proposal for future work are presented in section 5.

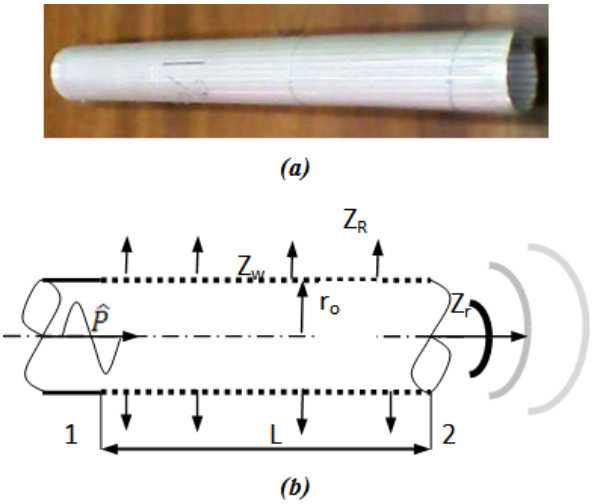

Figure 1. Geometry of the problem. a) Photo, (b) Contracture drawing

2. Theoretical Characterization of Perforated Duct

2.1. 1-D Based Theory

With the reference to Figure 1 and based on an earlier published paper by [8,9,10], the governing equations for 1D acoustic waves in this pipe are;

$$\frac{\partial \rho}{\partial t}+U_o\frac{\partial \rho}{\partial x}+\rho_o\frac{\partial u}{\partial x}=-\frac{4\rho_w}{d}u_w, \quad (1)$$

and

$$\rho_o\left(\frac{\partial}{\partial t}+U_o\frac{\partial}{\partial x}\right)u=-\phi_o\frac{\partial p_j}{\partial x}-\left(W_o-U_o\right)\frac{4\rho_w}{d}u_w \quad (2)$$

Here, ρ_o is density, p acoustic pressure, U_o mean flow speed, u acoustic velocity, W_o is the mean slip flow velocity at the pipe wall, $\phi=\left(1+\delta M_O^2\right)$, δ is a non-

dimensional parameter that depends on the mean flow profile, $M_o=U_o/c_o$ is the Mach number, and c_o is the speed of sound. The coupling between the fields in the inner of pipe and the outer atmosphere is done via side wall acoustic impedance.

$$Z_t = (p_1 - p_0)/u_w, \quad Z_t = \rho_o c_o z_t = \rho_o c_o (z_w + z_R) \tag{3}$$

To solve the problem a propagating wave is mathematically represented and harmonic space and time dependence are introduced. Suppressing the harmonic time dependence ($e^{i\omega t}$) the fluctuating quantities can then be written as;

$$p(x) = \hat{p}\, e^{-iKx},\ u(x) = \hat{u}\, e^{-iKx},\ \hat{p} = c_o^2 \hat{\rho}_o,\ \hat{p} = Z\ \hat{u} \tag{4}$$

Substituting equations (3) and (4) into equation (2) gives;

$$\rho_o c_o (ik_o + M_o(-iK)) Z^{-1} = i\phi_o K - \frac{(W_o - U_o)}{c_o} \frac{4\rho_w}{d\rho_o (z_w + z_R)} \tag{5}$$

where, $k_O = \omega / c_o$. Substituting equations (3) and (4) into equations (2) and with the help of equation (5), the characteristic wave impedance can be obtained;

$$Z = \frac{z_0 (k_0 - M_0 K)}{\phi K + 4iM_r \beta_o}, Z = \frac{z_0 (k_0 - M_0 K)}{\Phi K} \tag{6}$$

where, $\Phi = \phi K + 4iM_r \beta_O$, $\beta_o = \rho_\phi / D\rho_O (z_W + z_R)$, and $M_r = \frac{(W_o - U_o)}{c_O}$. Using equations (3) and (4) into equations (1) and with the help of equation (6) gives;

$$\frac{i\omega}{c_o^2} p + \frac{U_o}{c_o^2}(-iK)p + \frac{\rho_o(-iK)}{Z} p = -\frac{4\rho_w}{d\rho_o c_o (z_w + z_R)} p, \tag{7}$$

Simplifying equation (7), the axial wave number can be written as

$$k_o - M_o K - \frac{\Phi K^2}{(k_o - M_o K)} - 4i\beta = 0. \tag{8}$$

2.2. Acoustic Impedance of the Perforated Side Wall

Acoustic impedance normal to perforated side wall Z_w is explained as follows;

$$Z_W = Z_{MPP} + Z_R \tag{9}$$

Where Z_{MPP} is acoustic impedance of the perforated plate and it is calculated as;

$$z_{MPP} = (r_{MPP} + ix_{MPP}) \tag{10}$$

where $z_{MPP}= Z_{MPP}/\rho_o c_o$ is the normalized acoustic impedance, r_{MPP} is the normalized acoustic resistance, x_{MPP} is the normalized acoustic reactance, k is the wavenumber.

For the MPP type used here with slit like holes it was decided to use the impedance formula presented in Ref. [11,12,13], which can be summarized as follow, the normalized resistance can be written as;

$$r = \mathrm{Re}\left(\frac{j\omega t_P}{\sigma c_o} \left[1 - \frac{\tanh(k_S\sqrt{j})}{k_S\sqrt{j}} \right]^{-1} \right) + \frac{2\alpha R_S}{\sigma\rho_o c_o} + \frac{0.3 M_g}{\sigma} \tag{11}$$

and the normalized reactance can be written as;

$$x = \mathrm{Im}\left(\frac{j\omega t}{\sigma c_o} \left[1 - \frac{\tanh(k_S\sqrt{j})}{k_S\sqrt{j}} \right]^{-1} \right) + \frac{\delta\omega F_\delta}{\sigma c_o} \tag{12}$$

where, $k_s = d_h\sqrt{\omega/4\eta}$ is the Stokes number relating the slit width to the viscous boundary layer thickness, σ is the MPP porosity, M_g is the grazing flow Mach number, t_P is the MPP thickness and d_h is the slit width, α is 4 for sharp slit edges, $R_S = \sqrt{2\eta\rho_o\omega}/2$, the factor δ is the acoustic end correction for both side of the slit and put equal to $0.85d_h$ and $F_\delta = \left(1 + \left(12.6 M_g\right)^3\right)^{-1}$ is the flow effect on acoustic reactance. While Z_R is radiating acoustic impedance from the cylinder surface is calculated based on [14] as;

$$Z_R = \frac{iz_0 k_0}{K} \frac{H_0^2(Ka)}{H_1^2(Ka)}, \tag{13}$$

where, H is Hankel function.

2.3. Reflection Coefficient Education

With the reference to Figure 1 and based on the plane wave theory, the relation between the acoustic pressure and the volume velocity at cross section 1 and 2 can be represented as [15];

$$\begin{pmatrix} p_1 \\ q_1 \end{pmatrix} = \begin{pmatrix} T_{11} & T_{12} \\ T_{21} & T_{22} \end{pmatrix} \begin{pmatrix} p_2 \\ q_2 \end{pmatrix} \tag{14}$$

Where T is 2-port matrix, with the help of impedance at both sections, $Z_i = p_i/q_i = \eta_i Z_o$, i=1,2 the normalized impedance at cross section 1 can be calculated as

$$\eta_1 = \frac{(T_{11}\eta_2 + T_{12})}{(T_{21}\eta_2 + T_{22})} \tag{15}$$

where,

$$\begin{aligned} T_{11} &= -Z_p \frac{e^{iK_p L}}{(-Z_p + Z_m)} + Z_m \frac{e^{-iK_m L}}{(-Z_p + Z_m)}, \\ T_{12} &= Z_p Z_m \frac{e^{iK_p L}}{(-Z_p + Z_m)} - Z_p Z_m \frac{e^{-iK_m L}}{(-Z_p + Z_m)}, \\ T_{21} &= -\frac{e^{iK_p L}}{(-Z_p + Z_m)} + \frac{e^{-iK_m L}}{(-Z_p + Z_m)}, \\ T_{11} &= Z_m \frac{e^{iK_p L}}{(-Z_p + Z_m)} - Z_p \frac{e^{-iK_m L}}{(-Z_p + Z_m)}, \end{aligned} \tag{16}$$

where, Kp, Km are the axial incident and reflected wave number that are calculated from equation (8) using Newton Raphson method [16] and sample of the results are shown in Figure (2). Also, Zp, and Zm are the related calculated impedances from equation (6) based on the results from equation (8) and sample of the results are presented in Figure (3).

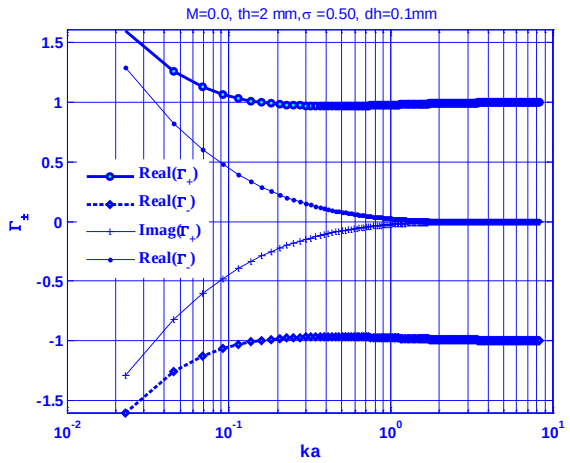

Figure 2. Propagation constant (Kp/k), (Km/k) versus Helmholtz number at M_o=0, Φ=1, ϕ=1.

The reflection coefficient magnitude can be calculated as

$$|R| = \left|\frac{\eta_1 - 1}{\eta_1 + 1}\right| \tag{17}$$

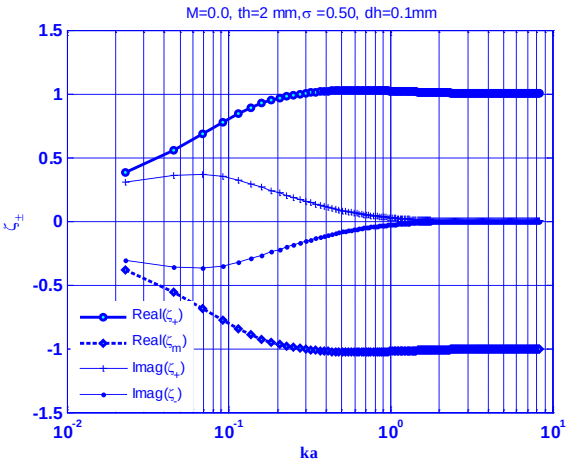

Figure 3. Specific impedances (Zp/zo), (Zm/zo) versus Helmholtz number at M_o=0, Φ=1, ϕ=1

Also, the power absorption coefficient can be calculated by

$$\alpha = 1 - |R|^2 \tag{18}$$

This represents the amount of incident sound energy absorbed by the presented (perforated) termination. The insertion loss can be also calculated using $IL = -10\lg(\alpha)$.

2.4. Sample of the Predicted Results

Since a subsonic low Mach number mean flow is of interest, $\delta M_o^2 \ll 1$, with less than about 1% error [5] and, consequently, this term is neglected in Equation (2) in the subsequent analysis i.e. ϕ≈1. The slip velocity, w_o, is kept as a model parameter in equation (6), in the current application it is eventually assumed to be very small compared to U_o to justify the assumption of $W_o/U_o \approx 0$, i.e., no-slip flow, with the boundary layer losses being neglected, it is has been found that it has negligible effect as well.

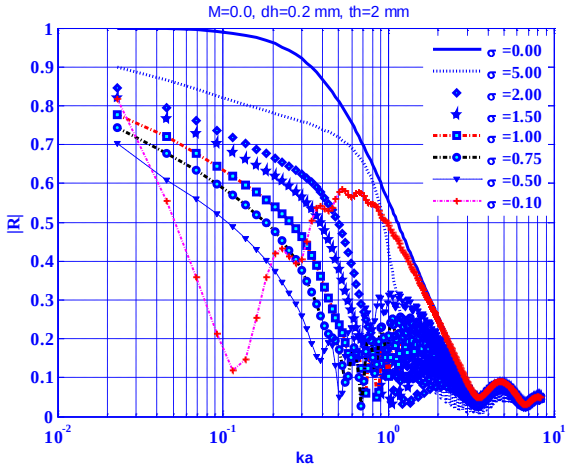

Figure 4. Effect of wall porosity on the system reflection coefficient using 500 mm MPP at the pipe outlet at Mo=0, Φ=1, ϕ=1

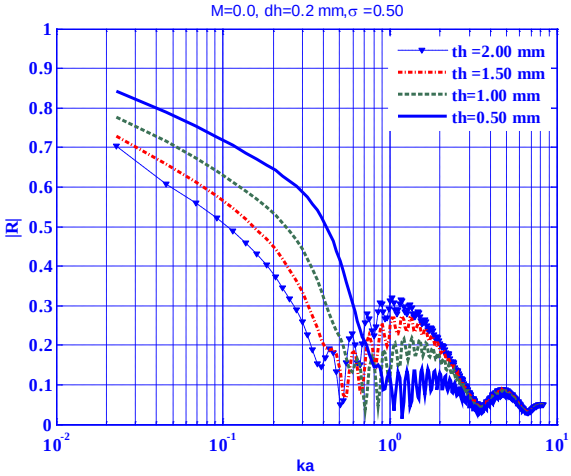

Figure 5. Effect of wall thickness on the system reflection coefficient using 500 mm MPP at the pipe outlet with M_o=0, Φ=1, ϕ=1

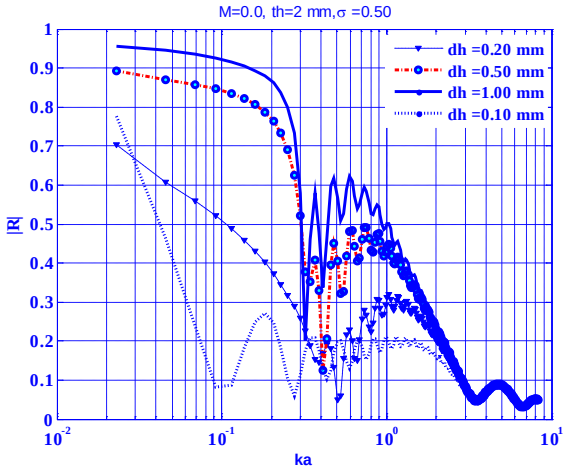

Figure 6. Effect of slit width on the system reflection coefficient using 500 mm MPP at the pipe outlet with M_o=0, Φ=1, ϕ=1.

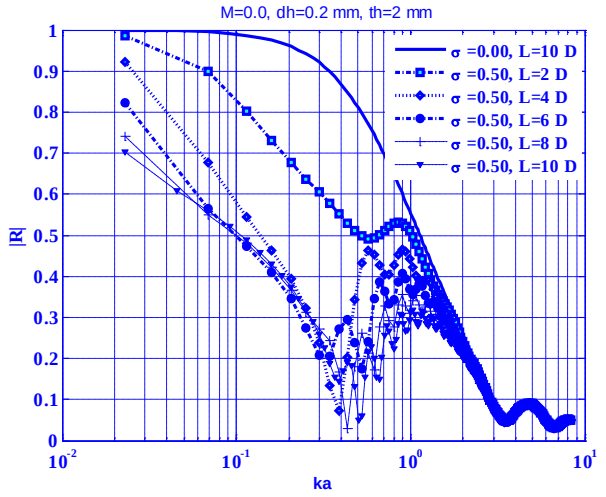

Figure 7. Effect of pipe length on the system reflection coefficient using MPP at the outlet

The effect of pipe wall porosity (σ) is presented in Figure 4, it can been that the lower porosity is better to reduce the system reflection (R) coefficient until it reaches σ ≈ 0.1%, R starts to increase again due to the increased of the wall impedance and behave like solid wall. The results related to σ ≈ 0.5% is quiet good in low frequency region and that related to σ ≈ 1% can be more efficient in the entire frequency rang. Based on the calculated results presented in Figure 5, the wall thickness of 2mm can be reasonable choice from acoustical and practice point of views. It can be also seen that the pipe, which manufactured of MPP with slit width (dh=0.1 mm) is effective but the reflection coefficient starts to increase at very low frequency as shown in Figure 6.

Figure 7 presents very interesting results which shows that even if the pipe length is twice the duct diameters, reasonable reduction in the reflection coefficient can be seen. It can be seen that, the reflection coefficient related to length of 4 - 6 that are mostly used in the vehicle application is very efficient.

Figure 8 (a), shows, the relation between the variations of the insertion loss versus Helmholtz number with different MPP pipe length. It can be seen also that IL increases with L/D due to the increase of the dissipation of acoustic energy. It can be also, summarize the L/D effect by using the level summation at each L/D using;

$$IL_S = 10\lg\left(\sum_{i=1}^{N} 10^{IL_i/10}\right) \tag{19}$$

Where N is the number of frequency points from 10 Hz to the cut-on frequency which is 4 kHz, i.e. ka=1.84. Summary of that values are presented in Table 1. The difference between the each case and the original L/D=0 or L/D=10 and σ=0 (with impermeable wall) is presented in Figure 8 (b).

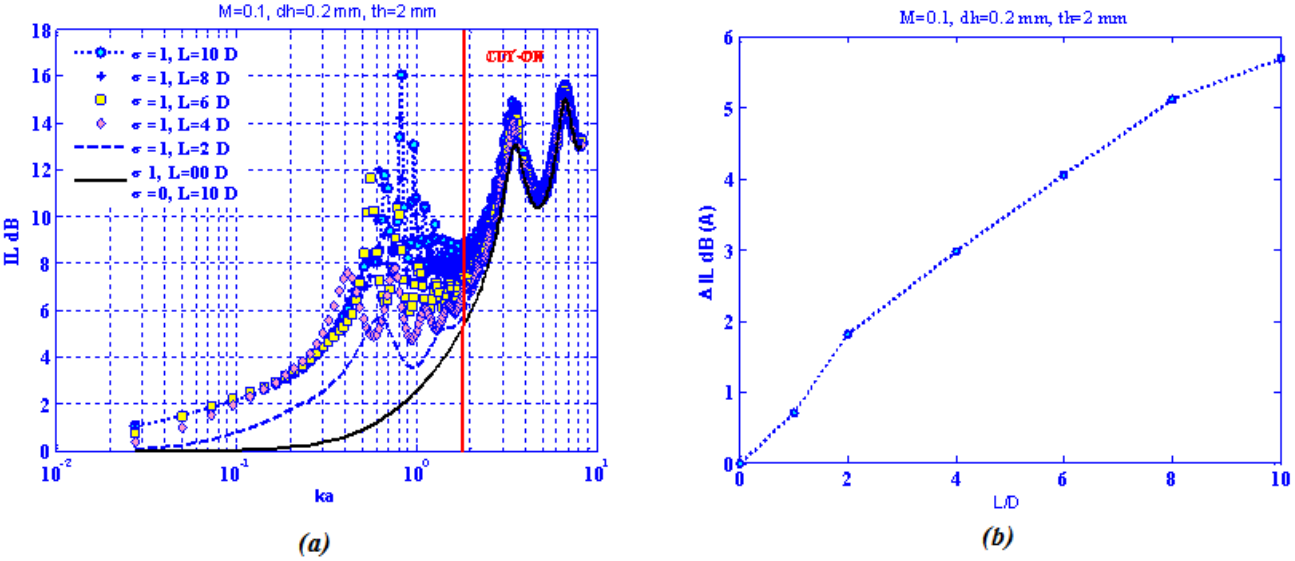

Figure 8. Variation of insertion loss versus perforated pipe length next to pipe open end. (a) IL versus ka, (b) IL difference versus L/D with and without MPP next to duct outlet

Table 1. Variation of summation of IL with L/D.

L/D	0	1	2	4	6	8	10
IL_sum	21.78	22.49	23.59	24.76	25.83	26.90	27.47

where, $\Delta IL_i = IL_{sum})_i - IL_{sum})_{L/D=0}$ and i=0,1,2,4,..,10.

2.5. 2-D Based Method

The acoustic wave equation for present test objects is given by [15];

$$\nabla^2 p - \frac{1}{c^2}\frac{\partial^2 p}{\partial t^2} = 0, \tag{20}$$

Using separation of variables, its time-harmonic solution in cylindrical coordinates yields the acoustic pressure field of normal modes inside a cylinder as;

$$p(r,\theta,x,t) = J_q(k_r r)e^{iq\theta}\left[Ae^{-ik_x x} + Be^{ik_x x}\right]e^{i\omega t}, \tag{21}$$

The radial and axial wavenumbers are related by

$$k_o = \sqrt{k_r^2 + k_x^2} \tag{22}$$

Acoustic pressure dependent on radial direction r is described by $J_q(k_r r)$, Bessel's function of the first kind of integer order q.

For a termination that contains absorption lining the inner circumference, it is assumed here that the wall is "local-reacting. The boundary condition at the absorbing surface located at r_0 (see Figure 1) is finite and Z_w is presented in equation (9),

$$\left.\frac{p}{u_r}\right|_{r=r_o} = Z_w, \tag{23}$$

where Z_w is the acoustic impedance normal to the wall surface and u_r is the particle velocity normal to the surface (acting in the radial direction).

The radial velocity is calculated by assuming a time-harmonic dependence in Euler's linear equation

$$u_r = -\frac{1}{i\rho\omega}\frac{\partial p}{\partial r}, \tag{24}$$

The pressure in the absorbing duct, assuming axisymmetric modes (i.e. m = 0), must be of the form

$$p(r,x,t) = J_0(k_r r)\left[Ae^{-ik_x x} + Be^{ik_x x}\right]e^{i\omega t}, \tag{25}$$

since the finite impedance at the absorbing wall implies $\partial p/\partial r$ is non-zero. This gives rise to the acoustic pressure having radial dependence.

$$(k_r r_o)\frac{J_1(k_r r_o)}{J_0(k_r r_o)} = ikr_o\frac{Z_o}{Z_w}, \tag{26}$$

where, the relationship $J_o'(k_r r_o) = -J_1(k_r r_o)$ was used [17]. The condition in Eq. (25) is a transcendental function whose roots are discrete values of $k_r r_o$ that satisfy the equation for each frequency dependent zw.

It applies only to modes for which m = 0. Since the specific acoustic impedance zw at the wall is complex, the roots will also be complex. Therefore, both radial and axial wavenumbers are complex quantities. This is to be expected since the imaginary part of the complex axial wavenumber is the attenuation constant of the duct. Determining the complex roots of Equation (26) is not trivial and it solved numerically using Newton Raphson Method for each frequency [16].

2.6. FEM Approach

2.6.1. General

For the numerical predictions the acoustic module of 3D FEM software COMSOL Multiphysics [18] has been used. Assuming a negligible mean flow the sound pressure p will then satisfy the Helmholtz equation:

$$\nabla\cdot\left(\frac{1}{\rho_o}\nabla p - \mathbf{q}\right) + \frac{k_o^2 p}{\rho_o} = 0 \tag{27}$$

where, the acoustic pressure is a harmonic quantity, $p = P_o e^{i\omega t}$, (N/m2). The **q** term (N /m^3) is a dipole source term corresponding to acceleration/unit volume which here can be put to zero.

In the current application, a vibrating piston is mounted inside one end of a cylindrical pipe. The other end is open connected to a PML (perfectly matched layer) region. The piston vibrates harmonically with a velocity where v_o = 1 m/s, and $\omega = 2\pi$ f is the angular frequency (rad/s). The model sweeps the frequency, f, through a range of values between 50 Hz and 15000 Hz. The acoustic medium is air with a density of 1.25 kg/m^3 and a speed of sound of 343 m/s. The axial symmetry of the geometry and the physics makes it natural to set the model up in a 2D axisymmetric application mode. Two cylindrical PMLs represent the air outside the pipe as shown in Figure 9.

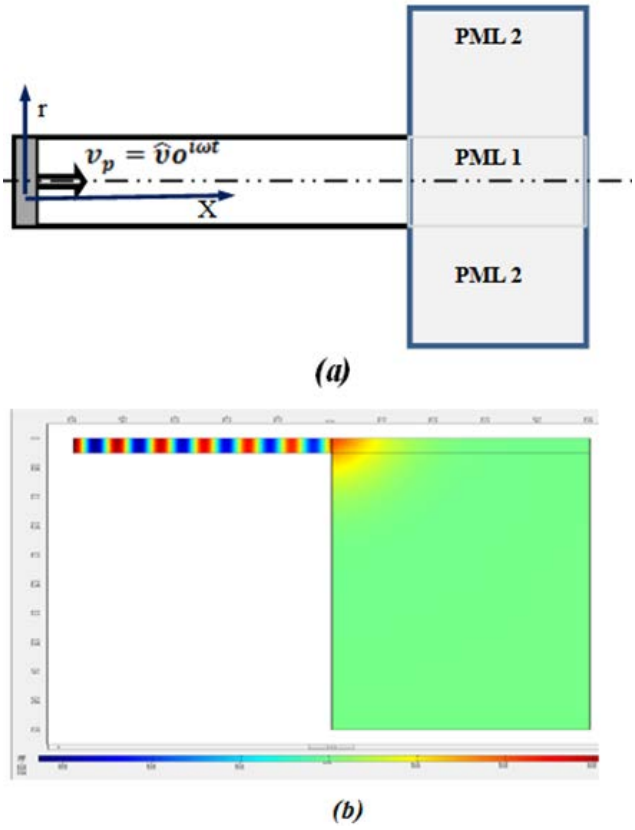

Figure 9. (a) Model geometry. PML 1 is damping only in the x direction, while PML 2 is damping in both the r direction and the x direction. (b) Surface pressure from FEM solution at 4kHz using Extra fine Mesh with 7148 elements. Pipe1 (r,z)=(0.025,0.5), Pipe2 (0.025,0.5), pipe3 (0.5,0.5)

2.6.2. Boundary Conditions

In this model three distinct boundary conditions are used. First, it represents the hard walls of the pipe by the equation

$$\nabla\cdot\left(\frac{1}{\rho_0}\nabla p - \mathbf{q}_S\right) = 0 \tag{28}$$

where **n** is the outward-pointing unit normal vector seen from inside the acoustics domain. The model also uses this condition at the exterior boundaries of the PMLs. Second, the piston is modelled with a normal acceleration condition:

$$\nabla\cdot\left(\frac{1}{\rho_0}\nabla p - \mathbf{q}_S\right) = a_n \tag{29}$$

where the normal acceleration, a_n, is defined as $i\omega v_0$. Third, the pipe wall impedance is modelled based on:

$$\nabla\cdot\left(\frac{1}{\rho_0}\nabla p - \mathbf{q}_S\right) = \frac{i\omega p}{Z_w} \tag{30}$$

The impedance Z_w is a function of the frequency obtained by equation (9).

The piston impedance $Z_p=p/v_o$ evaluated at the piston [19], introduce the quantities $z_p = \eta_p z_o$ Z_o where,

$$\eta_p = Z_p / z_o \tag{31}$$

where, η_p is the normalized piston impedance, z_o is the acoustic impedance of the air in the free field. Sample of the numerical calculation is compared with the 1D model is presented in Figure (10), which shows that in case of M=0 and σ=0, both results are identical. Also, there is very good agreement between them in case of M=0 and σ=0.5%. But, very small deviation can be seen at M=0.1 and σ=0.5% because the convective flow effect is neglected in main duct FEM is used but it is effect on wall impedance is add [20].

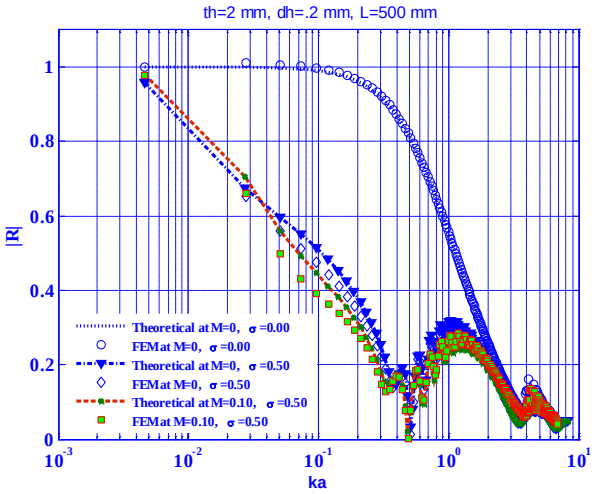

Figure 10. Predicted reflection coefficient using presented theories and FEM with and without flow.

3. Experimental Verification

3.1. Plan Wave Representation

Wave propagation in the straight hard walled ducts below the first cut-on frequency, can be treated as plane wave type and the acoustic pressure can be expressed as [21,22]

$$p(x,t) = p_+(t - x/c) + p_-(t + x/c) \tag{32}$$

here, p is the acoustic pressure, c is the speed of sound, x is the position along the x-axis. Since at low frequencies the sound field can be completely determined by simultaneous pressure measurements at two axial positions along the duct, the sound field can then be expressed as a function of frequency domain as:

$$\hat{p}(x, f) = \hat{p}_+(f)\exp(-ik_+x) + \hat{p}_-(f)\exp(ik_-x) \tag{33}$$

and

$$\hat{u}(x, f) = \frac{1}{\rho c}[\hat{p}_+(f)\exp(-ik_+x) + \hat{p}_-(f)\exp(ik_-x)] \tag{34}$$

where $\hat{p}$ is the Fourier transform of the acoustic pressure, $\hat{u}$ is the Fourier transform of the particle velocity, x is the coordinate along the duct axis, f is the frequency, k is the complex wavenumber denotes propagation in positive and negative x-direction, r is the density and c is the speed of sound.

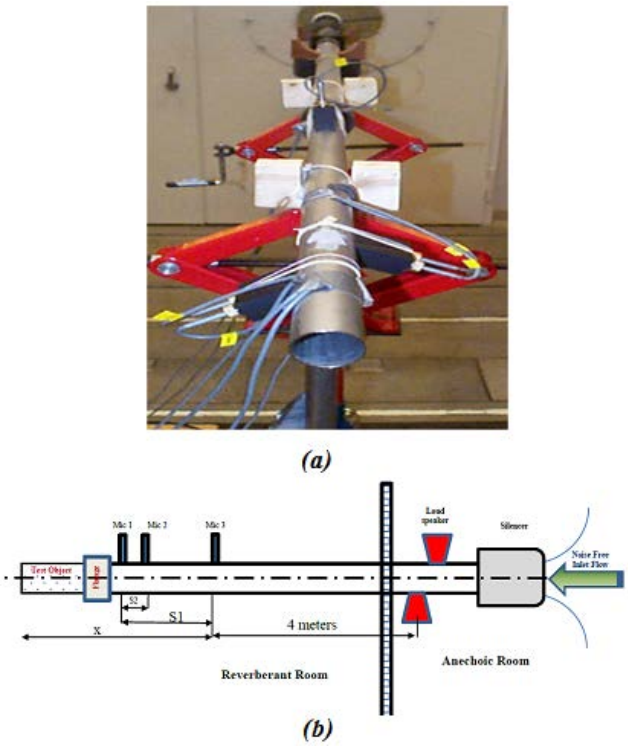

Figure 11. Measurement setup of the Two-Microphone Method, a) Photo, b) Contracture drawing

3.2. Reflection Coefficient Measurement Procedure

By assuming the complex wavenumbers are known in the duct, the incident and reflected wave amplitudes $\hat{p}_+$ and $\hat{p}_-$ can be calculated using two microphone positions as shown in Figure 11.

Using Equation (34) at x=0 with reference microphone gives;

$$\hat{p}_1(x, f) = \hat{p}_+(f) + \hat{p}_-(f) \tag{35}$$

And at x=s gives;

$$\hat{p}_2(x, f) = \hat{p}_+(f)\exp(-ik_+s) + \hat{p}_-(f)\exp(ik_-s) \tag{36}$$

where, s represents the microphone separation. Equation (35) and (36) imply that

$$\hat{p}_+(f) = \frac{\hat{p}_1(f)\exp(-ik_+s) - \hat{p}_2(f)}{\exp(ik_-s) - \exp(-ik_+s)} \tag{37}$$

and

$$\hat{p}_-(f) = \frac{-\hat{p}_1(f)\exp(-ik_+s) + \hat{p}_2(f)}{\exp(ik_-s) - \exp(-ik_+s)} \tag{38}$$

Equations (37) and (38) are the basic TMM equations from which all plane wave quantities of interest can be calculated. To use these equations in practice it is firstly necessary to compensate for the amplitude and phase shift associated with each microphone channel. Secondly, with flow in the duct it is necessary to improve the signal-to-noise ratio by using the source signal (loudspeaker voltage) as a reference. If it assumed that the duct has a linear and

passive termination in the positive x-direction a reflection coefficient can be defined in that direction

$$R(f) = \hat{p}_- / \hat{p}_+ \tag{39}$$

Åbom and Boden [23] proved that the TMM has its lowest sensitivity to errors in the input data in a region around $ks = \frac{\pi(1-M^2)}{2}$, where M is the Mach number. They also stated that to avoid large sensitivity to the errors in the input data, the two-microphone method should be restricted to the frequency range as $0.1\pi(1-M^2) < ks < 0.8\pi(1-M^2)$ where M is the Mach number.

Measurements were performed using the flow acoustic test facility available at The Marcus Wallenberg Laboratory, Department of Aeronautical and Vehicle Engineering at KTH, Sweden. A circular steel pipe of inner diameter 50 mm with a wall roughness of less than 0.1 mm, and inner diameter 50 mm was used. In the pipe the 3 quarter inch microphones (B&K 4938) were flush mounted at the positions shown in Figure (11). The first measurement position x1 was fixed at 650 mm from the open end. At room temperature the cut-on frequency of the first higher-order mode in the test pipe is approximately 4.0kHz.Two loudspeakers connected to the pipe via short side branches provided the acoustic excitation. The loudspeaker sections were placed in an anechoic room and a dissipative silencer was used to remove reflections from the upstream termination, together with a very smooth conical diffuser which also provided a low-noise inlet flow. The unflanged opening of the pipe was placed in the middle of a reverberant room, 1.5 m above a rigid floor. The nearest wall was 2.5 m from the pipe open end. Careful attention was taken to avoid flow-induced vibrations of the pipe by using soft supports.

The microphones were flush-mounted and a source correlation technique [24,25] with stepped sine excitation was adopted to suppress the flow-generated noise and get a good signal-to-noise ratio. To improve the quality of the measurement the 500 averages has been used. The measurements were repeated three times and the average values were used in the final analysis. The first test was performed for steel pipe, and the last 500mm of the pipe is replaced by pipe with permeable wall, which has wall thickness 1mm, porosity of, and slit width of 0.2 mm.

3.3. Relation between Predicted and Measured Reflection Coefficient

Comparison between the measured and predicted results is presented in Figure 12(a) without flow and with flow in Figure 12(b). From these results it can be seen that the measured results agree with the predicted results using a 1D, 2D and FEM at M=0, but there is some small deviation at M=0.1 may be due to the neglecting convective effect with FEM prediction. 2D based solution gives the best results compared with the measurements but it is more time consuming than 1D solution.

Increasing the flow Mach number reduce the reflection coefficient because it partially block the MPP holes and increase the wall impedance as shown in equation (11). This makes it even useful to use the MPP as a snorkel in the intake system.

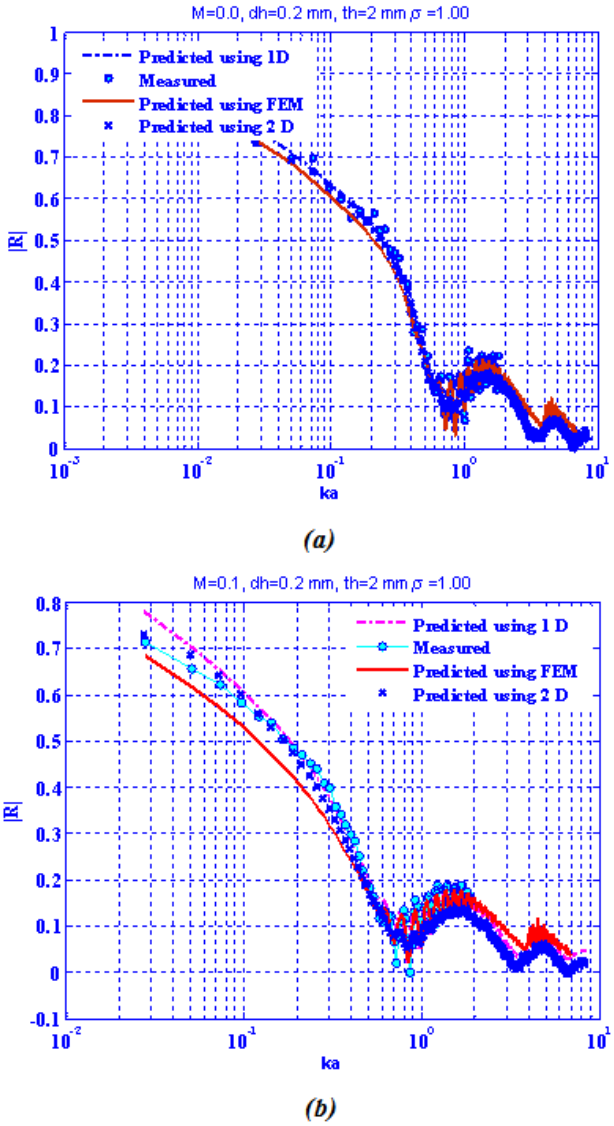

Figure 12. Comparison between predicted and measured reflection coefficient using presented theory and FEM. (a) M=0, (b) M=0.1

3.4. Real Application

The proposed acoustic element is used as a tail pipe with two different passenger cars (Toyta Model 2015 and Shahin Model 2005) and both are popular in Egypt with 6D in length i.e. L/D= 6, where D is the inner duct diameter 50 mm. The radiated noise is measured using the RO-line precision sound level meter (SLM) type 1350 based on and the background noise (free field) is 30 dB lower than the measured sound pressure level (SPL) from the source under test [26]. The measured data are collected at different engine speeds ranging from 500 to 6000 rpm without load. The Sound level meter is fixed at 0.5 m away from the exhaust system outlet and 1 meter over the ground surface, i.e. in (x,y,z) = (0.5,0.5,1.0) with inclination of 45° as shown in Figure 13.

The measurements are repeated three times and the average values are used. Also, the average values of both vehicles are calculated and used in this analysis. The SPL difference between the existed tail pipe, which has a hard

wall with 2mm thickness and proposed one, is presented in Figure 14.

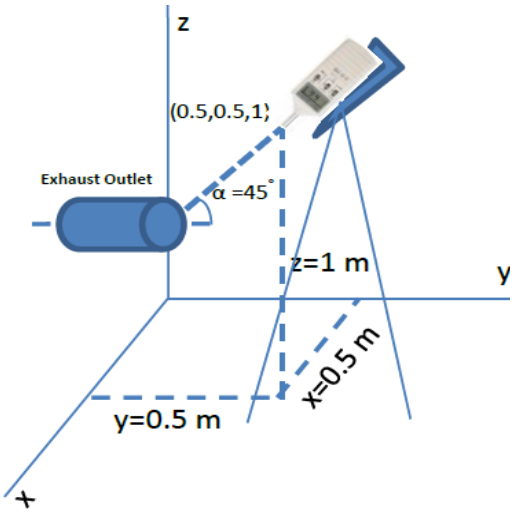

Figure 13. Position of SLM during the measurements

By comparing the results presented in Figure 14 with that presented in Figure 8(b), It can be seen that 5 dB(A) can be achieved at 3000 rpm, and in general the average sound reduction can be 4.1 dB(A). By comparing this result with that presented in Figure 8(b) at L/D=6 which gives 4 dB(A) that means the simulation is in a very good agreement with the measurements.

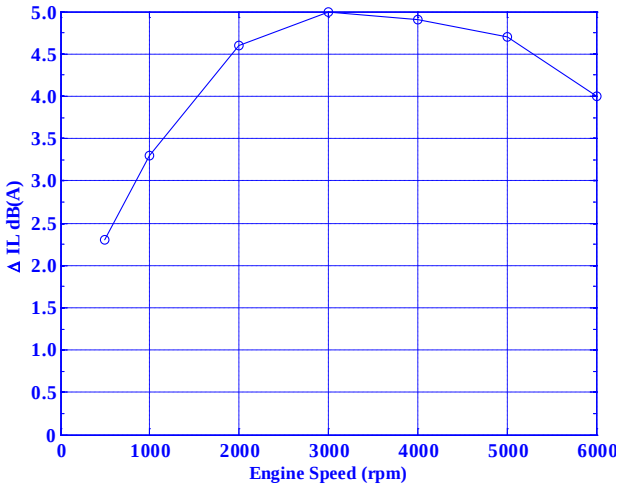

Figure 14. SPL difference versus engine speed for vehicle 1 at no load.

4. Conical Outlet Shape

The procedure presented in section 2.1 can be applied to the preferable conical outlet shape that is shown in Figure 15, directly if the total length of the cone is divided into several straight ducts with length small enough compared with the wave length. The 2-port of the cone is calculated by multiplying the 2-port of all straight ducts at each certain duct diameter. The 2-port can be also calculating using the following equation [17] and the reflection coefficient is calculated using equation 41 with equation 16 and 18.

$$\begin{bmatrix} p_1 \\ u_1 \end{bmatrix} = \begin{bmatrix} T_{11} & T_{12} \\ T_{21} & T_{22} \end{bmatrix} \begin{bmatrix} p_2 \\ u_2 \end{bmatrix} \tag{40}$$

Where

$$T_{11} = \frac{x_2}{x_1}\cos(k_o l) - \frac{1}{k_o x_1}\sin(k_o l),$$

$$T_{12} = jZ_d \frac{x_2}{x_1}\left(\sin(k_o l)\right),$$

$$T21 = \frac{j}{Z_d}\left\{\begin{array}{l} \frac{x_1}{x_2}\left(1+\frac{1}{k_o^2 x_1 x_2}\right)\sin(k_o l) - \\ \left(1-\frac{x_1}{x_2}\right)\frac{\cos(k_o l)}{k_o x_2} \end{array}\right\}, \tag{41}$$

$$T_{22} = \frac{1}{k_o x_2}\sin(k_o l) + \frac{x_1}{x_2}\cos(k_o l).$$

here $x_1 = \frac{r_1}{r_2 - r_1}L$, $L = x_2 - x_1$ and $Z_2 = \frac{\rho_o c_o}{\pi r_2^2}$. Detail analysis for conical shape dimension calculation is presented in Appendix A.

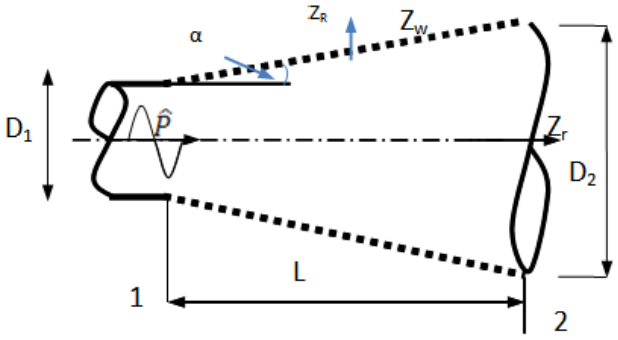

Figure 15. Flow distribution and the acoustic waves in the test object

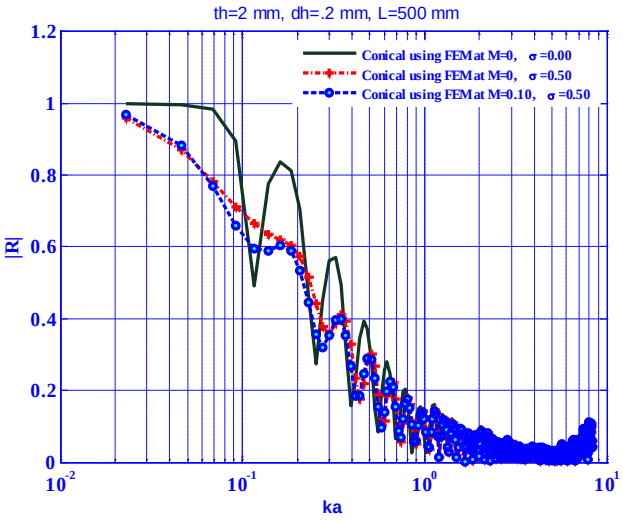

Figure 16. Effect of porosity on the reflection coefficient using cone MPP at the outlet, L= 500 mm, D1=50 mm, D2=195 mm, Θ=16.5°

Table 2. Conical Outlet Dimensions.

Case	D1 mm	D2 mm	L mm	X1 mm	X2 mm	Θ °
A	50	195	500	173.6	673.6	16.5
B	50	93.7	500	570	1070	5

In this case since, it has been found that all models are almost the same time consuming around 600 sec and all are working quite well in the frequency range of interest from (10 to 4000 Hz), the FEM solution is used with 35000 elements, and fine mesh, see Appendix A for more

details. Figure 16 shows the effect of porosity on reflection coefficient with and without flow using the same pipe length, 500 mm and the same inlet diameter, while the other dimensions are presented Table 2. It is clear from the figure that wall porosity reduces the sound reflection coefficient.

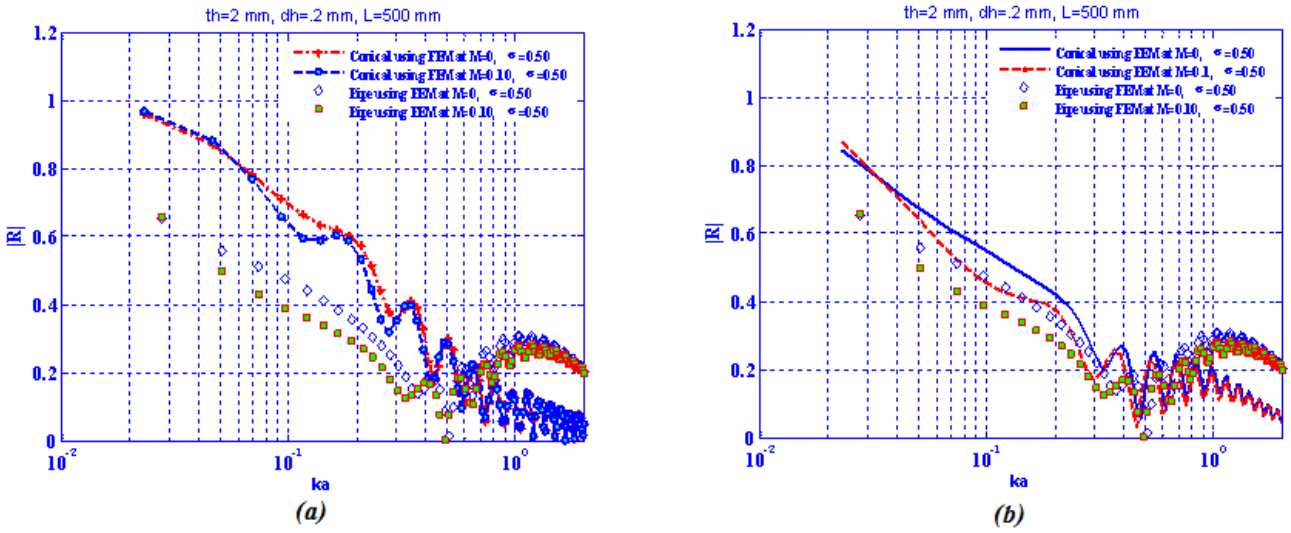

Figure 17. Effect of outlet shape on the sound reflection coefficient. (a) conical Case A, (b) conical case B, shown in Appendix A

Comparison between the conical outlet and pipe with the same length, and the same inlet diameter is presented in Figure 17, which shows that the pipe with permeable wall is better to reduce the sound reflection coefficient at low Helmholtz ka≤0.5 number while the cone is better at higher Helmholtz number. Even if the cone outlet diameter is reduced still the same results can be seen from Figure A1.

5. Conclusion

In this paper, reflection coefficient |R| and noise reducing due to perforated/micro perforated side wall at a duct open end was studied analytically, numerically and experimentally. The following conclusions were obtained:

Two analytical models of the perforated side wall at a duct open end was constructed; one based on 1D wave equation and the other based on 2D wave equation, and they show that properly designed perforation remarkably reduce sound reflection coefficient of the duct and radiated sound from the exit. FEM based on a 3D acoustic module in Comsol Multiphysics is also constructed and its results are compared with the previous models and they are in a very good agreement. These models are validated by induct measurements at room temperature and the results are in a very good agreement.

The effects of all design parameters on the sound reflection coefficient are presented. The results show the reduction of |R| and the improvement of IL not only depends on the length of MPP pipe at the outlet but also its acoustic impedance.

This investigated element is used to reduce low frequency sound radiated from passenger car as a tail pipe with L/D=6, and It gives 4 dB(A) reduction in average with engine speed, which represented 6% of the total radiated sound. To make the conical shape more efficient at small ka, its length must be increased.

For future work and based on these results one can try to optimize the outlet acoustic performance and space and shape constrains.

Acknowledge

Author would like to thank all Flow Acoustic Group at MWL, the Aeronautical and Vehicle Engineering Department, KTH, Stockholm, Sweden for all supports during measurements and useful and interesting discussions.

References

[1] R.M. Munt, “Acoustic transmission properties of a jet pipe with subsonic jet flow, I: the cold jet reflection coefficient”. Journal of Sound and Vibration 142 (3) (1990) 413-436.

[2] J. M. Egana, J. Diaz, J. Vinolas, *Active control of low-frequency broadband air conditioning duct noise*, Noise Control Eng. 51 (5) (2003) 292-299.

[3] G. F. KUHN and C. L. MORFEY 1976 Journal of Sound and Vibration 47, 147-161. Transmission of low-frequency internal sound through pipe walls.

[4] A. CUMMINGS 1983 Journal of Sound and Vibration 90, 193-209. Higher order mode acoustic transmission through the walls of rectangular ducts.

[5] R. J. ASTLEY and A. CUMMINGS 1984 Journal of Sound and Vibration 92, 387-409. A Fnite element scheme for acoustic transmission through the walls of rectangular ducts: comparison with experiment.

[6] A. CUMMINGS and R. J. ASTLEY 1995 Journal of Sound and Vibration 179, 617-646. The effects of flanking transmission on sound attenuation in lined ducts.

[7] A. CUMMINGS AND R. KIRBY Journal of Sound and Vibration (1999) 226(2), 237-25. 1LOW-FREQUENCY SOUND TRANSMISSION IN DUCTS WITH PERMEABLE WALLS.

[8] E. Dokumaci, Effect of sheared grazing mean flow on acoustic transmission in perforated pipe mufflers, Journal of Sound and Vibration 283 (2005) 645-663.

[9] M. L. Munjal, *Acoustics of ducts and mufflers*, Chichester: John Wiley, 1987.

[10] Allam S. and Abom M., 2011, ‘‘A New Type of Muffler Based on Micro perforated Tubes’’. Journal of Vibration and Acoustics’’, ASME Journal of Vibration and Acoustics, 133.

[11] D.-Y, Maa. *Potential of microperforated panel absorber*, Journal of Acoustical Society of America, Vol.104, no.5, July 1998.

[12] Allam, S., and Åbom, M., 2008, "*Experimental Characterization of Acoustic Liners With Extended Reaction*," The 14th AIAA/CEAS Conference 2008, p. 3074.

[13] J. Liu, D. W. Herrin and A. F. Seybert "*Application of Micro-Perforated Panels to Attenuate Noise in a Duct*" SAE 2007-01-2196.

[14] Robert D. Skorheim "On the radiation impedance of an array of finite cylinders". MSc thesis in Engineering Electronics. United States Uaval Postgraduate School. Monterey, California, Jan 1957. Report No. AD00479606.

[15] Uno Ingard "NOISE REDUCTION ANALYSIS". World Headquarters. Jones and Bartlett Publishers. ISBN: 978-1-934015-31-5.

[16] G. Dahlquist, Å. Björck, N. Anderson, Numerical Methods, Prentice-Hall, Englewood Cliffs, NJ, 1974.

[17] Fridolin P. Mechel "*Formulas of Acoustics*" Second Edition. Springer-Verlag Berlin Heidelberg New York 2008. ISBN: 978-3-540-76832-6

[18] *COMSOL Multiphysics 3.5a*, User's Guide Copyright 1994-2010.

[19] P.M. Morse and K.U. Ingard, Theoretical Acoustics, Princeton Univ. Press, 1986.

[20] Elnady, T. Åbom, M. Allam, S. "Modeling perforates in mufflers using two-ports". ASME, Journal of Vibration and Acoustics, 2010. Vol. 132 / 061010-1-11.

[21] ISO 10534-1, Acoustics — Determination of Sound Absorbing Coefficient and Impedance in Impedance Tubes, Part I: Method Using Standing Wave Ratio, 1996.

[22] ISO 10534-2, Acoustics — Determination of Sound Absorption coefficient and Impedance method in Impedance Tubes, Part II: Transfer - Function method, 1998.

[23] M. Åbom, H. Boden, Error analysis of two-microphone measurements in duct with flow, Journal of Acoustical Society of America 83 (1988) 2429-2438.

[24] M. Åbom, "*Measurement of the scattering matrix of acoustical two-ports*," Journal of Mechanical System and Signal Processing 5 (1991) 89-104.

[25] Sabry Allam, Mats Åbom "Investigation of damping and radiation using full plane wave decomposition in ducts". Journal of Sound and Vibration 292 (2006) 519-534.

[26] Lief, N. "*International standards for acoustics and noise control*" .J. Noise Control Engng, March–April 1989, 32(2), 67-72.

Appendix A

Conical Outlet Specifications

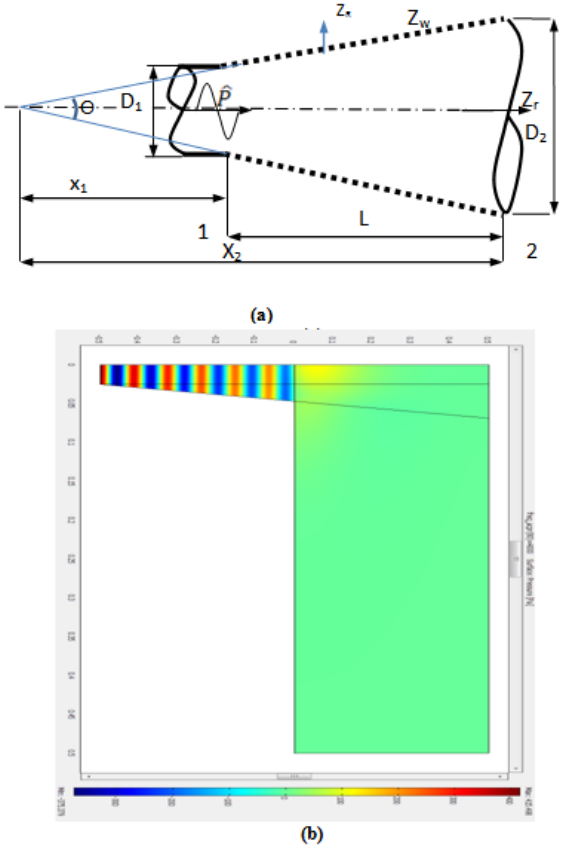

Figure A1. (a) Model geometry. PML 1 is damping only in the x direction, while PML 2 is damping in both the r direction and the x direction. (b) Surface pressure from FEM solution at 4kHz using Extra fine Mesh with 35000 elements. Dimension of case B in Table 2